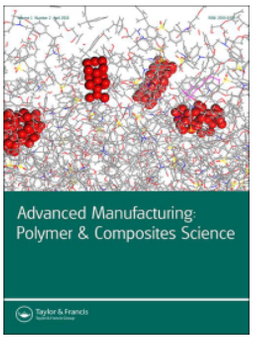

Taylor & Francis
Taylor & Francis Group

Advanced Manufacturing: Polymer & Composites Science

ISSN: 2055-0340 (Print) 2055-0359 (Online) Journal homepage: www.tandfonline.com/journals/yadm20

Strain distributions for tensile and shear loading around multiple holes in a thermoplastic composite introduced by thermally assisted piercing

Faranak Bahrami, Chris Worrall, John Watts, Matthew Oldfield, Stephen Ogin & Mihalis Kazilas

To cite this article: Faranak Bahrami, Chris Worrall, John Watts, Matthew Oldfield, Stephen Ogin & Mihalis Kazilas (2026) Strain distributions for tensile and shear loading around multiple holes in a thermoplastic composite introduced by thermally assisted piercing, Advanced Manufacturing: Polymer & Composites Science, 12:1, 2619999, DOI: 10.1080/20550340.2026.2619999

To link to this article: https://doi.org/10.1080/20550340.2026.2619999

Published online: 24 Jan 2026.

ADVANCED MANUFACTURING: POLYMER & COMPOSITES SCIENCE
2026, VOL. 12, NO. 1, 2619999
https://doi.org/10.1080/20550340.2026.2619999

Taylor & Francis
Taylor & Francis Group

RESEARCH ARTICLE

OPEN ACCESS Check for updates

Strain distributions for tensile and shear loading around multiple holes in a thermoplastic composite introduced by thermally assisted piercing

Faranak Bahrami[a,b,c], Chris Worrall[a], John Watts[b], Matthew Oldfield[b], Stephen Ogin[b] and Mihalis Kazilas[a,c]

[a]Non-Metallic Materials, TWI Ltd., Cambridge, UK; [b]Department of Mechanical Engineering Sciences, University of Surrey, Guildford, UK; [c]College of Engineering, Design, and Physical Sciences, Brunel Composites Centre, Brunel University London, London, UK

ABSTRACT

A multiple thermally assisted piercing process has been developed as a method of making equally spaced holes in thermoplastic composites. The consequences for the mechanical properties of the composite of introducing a limited set of inline holes into cross-ply laminates have been investigated. Open-hole tension and Iosipescu shear testing has been carried out on specimens containing drilled or pierced holes aligned with the direction of loading; microscopy and digital image correlation techniques have also been used to investigate local changes in fiber orientation and strain distributions under load. The strain fields for inline holes in drilled and pierced specimens under tensile loading can be understood in terms of local changes to the modulus as a consequence of the piercing or drilling process; in addition, some features of the strain fields can be predicted with the aid of a shear–lag model developed for modeling matrix cracking in cross-ply laminates. Although significant differences were found between the strain fields of the drilled and pierced specimens, no consistent improvement in strength was observed for the pierced composites compared to drilled composites for different holes spacings. Under shear loading, the pierced composites were found to have a significantly poorer response compared to drilled composites, which is related to the premature collapse of the holes in shear due to (a) localized fractures in regions of low fiber volume fraction and (b) intact fibers being pulled across the holes causing hole collapse.

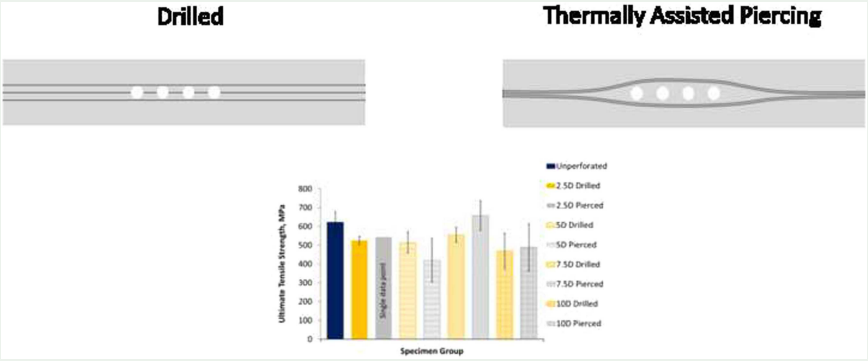

ARTICLE HISTORY
Received 24 October 2025
Accepted 16 January 2026

KEYWORDS
Drilled holes; machining; mechanical properties; open-hole; thermally assisted piercing; thermoplastic; Iosipescu; digital image correlation

1. Introduction

Composite parts can be manufactured to near-net-shape with minimum wastage of material; however, there is almost always a need for further machining. The most common post-manufacture machining operation for composite materials is hole creation, which accounts for approximately 90% of the aerospace industry's composite machining requirements [1]. The holes are primarily used for joining applications,

CONTACT Faranak Bahrami faranak.bahrami@brunel.ac.uk College of Engineering, Design, and Physical Sciences, Brunel Composites Centre, Brunel University London, Uxbridge, UB8 3PH, UK

although they may also be used for acoustic damping (e.g. in gas turbine engine nacelles or landing gear), leading edge deicing, and hybrid laminar flow control [2,3].

Drilling composites is heavily used in industry, as it is a relatively inexpensive method of machining holes (in comparison to laser or water-jet cutting) and can be used on large, non-flat structures without significant complications. However, if the drilling parameters are not carefully selected and controlled, delamination, fiber pull-out and fiber break-out can result from the drilling process [4–8], leading to a reduction in the mechanical performance of the composite material [9]. Drilling-induced damage and surface quality are known to influence the performance of composite laminates, and machining parameters are therefore commonly selected to minimize delamination and other drilling-related defects [10]. Difficulties in the accuracy and repeatability of the drilling can also lead to expensive part rejections. For example, Airbus delayed the entry-to-service date of the A350 XWB by three months due to difficulties in implementing the automated drilling process [11], which highlights the major complexity of drilling composites.

As an alternative to a material removal process such as drilling, material displacement processes, including moulded-in holes can be employed. Such material displacement approaches are particularly attractive for thermoplastic composite systems, which offer manufacturing and lifecycle advantages, including the potential for efficient joining and repair [12]. Several studies [13–20] have investigated the performance of the moulded-in holes in a composite material under tensile loading. The studies reported significant increases in tensile strength, which are a consequence of fiber continuity and local increases in the fiber volume fraction close to the holes [13–20].

In the most recent study [21], thermally-assisted piercing (TAP) was used, which is based on a material displacement process and is similar to moulded-in holes in the sense that holes can relatively easily be formed in a thermoplastic composite at various stages of manufacture. The study [21]. carried out open-hole tension and compression tests on TAP and drilled specimens, using a single 6.0 mm diameter hole, and found an improved open-hole tensile strength of 1%–10% (based on 3 processing temperatures) for the TAP specimens in comparison to drilled specimens. The open-hole compression results showed a 12% and 4% improvements in the TAP specimens in comparison to the drilled specimens for two of the smallest heated areas. However, the largest heating area (12 mm diameter) results indicated a 79% decrease in compressive strength for the TAP specimens in comparison to the drilled specimens, indicating that the processing parameters can have a significant effect on the mechanical properties of the TAP specimens.

The behavior of the specimens with a single moulded-in or pierced hole is interesting. However, in practice, multiple holes are often required, and this paper investigates the mechanical properties of multiply pierced composites where the piercing has been carried out using the TAP process.

2. Experimental methods

2.1. Specimen manufacture

Carbon fiber-reinforced polyamide-12 (PA12), hereafter referred to as CF/PA, pre-impregnated uni-directional tape (Suprem T55% AS4/PA12-2150; nominal fiber volume fraction and ply thickness of 0.55 and 0.15 mm, respectively), has been used to manufacture 16-ply laminates with configuration $[0/90]_{4s}$. The laminates were pressed at 214 °C (at a rate of 5 °C/min) under a consolidation force ramped at 0.5 kN/min to a final force of 9 kN corresponding to a consolidation pressure of 56 kPa over a 400 mm × 400 mm laminate, following the manufacturer's recommendation. After reaching the desired pressure and temperature, the conditions were maintained for an additional 25 min. The laminate was subsequently cooled down under the consolidation pressure to room temperature at an approximate cooling rate of 5 °C/min. The process produced a laminate with a nominal thickness of 2.4 mm (measured after manufacture).

Unperforated, drilled, and pierced specimens were subjected to open-hole tensile (OHT) and Iosipescu tests to determine the response to mechanical loading. For OHT testing, the specimen dimensions were 300 mm (length), 36 mm (width), and 2.4 mm (thickness). For the OHT specimens (drilled and pierced specimens), the diameter, D, and number of holes were the same, i.e. 2 mm hole diameter, with four holes aligned with the direction of the applied loading and the center-to-center hole spacing was varied in order

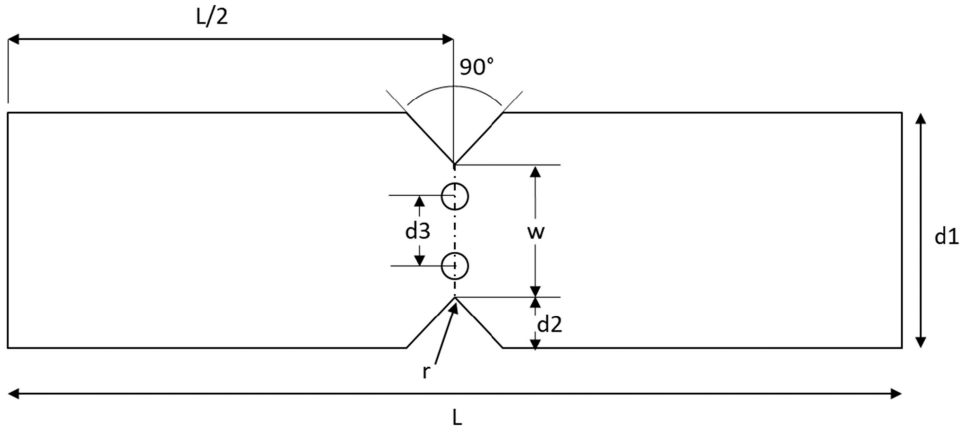

d1 = 19 mm; d2 = 3.8 mm; d3 = 5.00 mm; L = 76 mm; r (radius) = 1.3 mm; w = 11.4 mm

Figure 1. Iosipescu specimen dimensions.

to investigate the effect of the hole spacing on the mechanical properties. Hole spacings of 5 mm (i.e. 2.5D), 10 mm (i.e. 5D), 15 mm (i.e. 7.5D), and 20 mm (i.e. 10D) were used (where D is the hole diameter of 2 mm). Aluminium tabs (50 mm in length) were adhesively bonded onto the OHT specimens using Araldite 2014-2 (RT cure) with a bond line thickness of 1 mm (controlled with a jig). Some specimens required re-tabbing after the tabs failed at very low loads, before any damage was sustained by the specimen; the specimen and aluminium tabs were abraded and plasma treated before rebonding. For the Iosipescu tests, holes with a center-to-center spacing of 5 mm were tested, but the dimensions of the specimen enabled only two holes to be accommodated across the width of the specimen (see Figure 1).

With respect to producing the holes themselves, the drilled holes were manufactured using an interpolation technique; interpolation or 'helical interpolation' is a milling technique that can be used as an alternative to drilling [22]. The drilled holes were produced by a technical workshop using a CNC-controlled helical interpolation technique. Although the machining parameters (e.g. spindle speed and feed rate) were not recorded as part of the present study, it was specified that identical drilling parameters were used for all drilled specimens to ensure consistency. The selection of machining parameters was carried out by experienced technical staff using the established best practices for composite materials. The present study did not aim to investigate the influence of drilling parameters on hole quality or mechanical performance; rather, the interpolation technique was selected to achieve the highest possible and most consistent hole quality for comparison with the pierced specimens.

For the TAP specimens, the laminates were pierced in advance of machining the specimens to their final dimensions. To produce specimens with holes that were manufactured at the same time and in-line, a multiple-piercing TAP rig was designed and built (Figure 2). The piercing pins were manufactured from a 2 mm diameter silver steel rod, cut to a length of 13 mm and ground to a pointed tip. The influence of pin tip geometry was not investigated in this study, as previous work has shown that tip shape has no measurable effect on the strength of pierced composite specimens [21].

The composite laminate was clamped between aluminium plates and heated using a metal frame to a target temperature of 200 °C, above the melting point of the PA12 matrix. Once this temperature was reached, a dwell time of approximately 20 minutes was applied to allow thermal stabilization of the composite and tooling prior to piercing. The piercing process was then performed using a mechanical press without instrumented force or displacement measurement. Following piercing, the pins were retained within the laminate until the temperature of the metal frame reached room temperature in order to minimize relaxation during cooling; the temperature was monitored using an infrared thermal camera measuring the surface temperature of the metal frame.

The rig has the potential to pierce one hundred holes with a diameter of 2 mm simultaneously, with the flexibility of changing the hole spacing and pattern; an image of the rig fully-loaded with piercing pins is

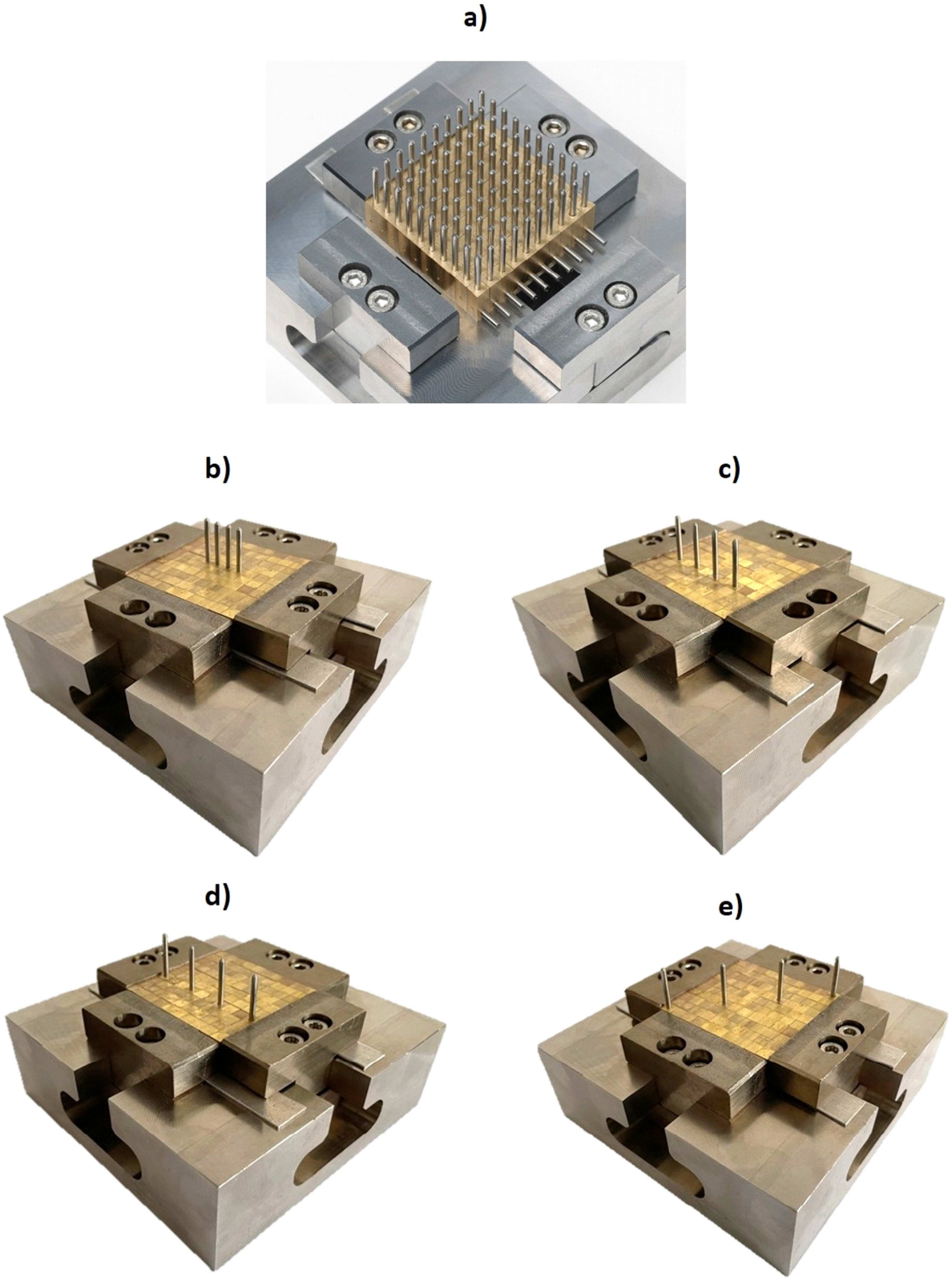

Figure 2. Multiple thermally assisted piercing rig for (a) fully loaded rig (not used in the current work); (b) hole spacing 5 mm; (c) hole spacing 10 mm; (d) hole spacing 15 mm; (e) hole spacing 20 mm.

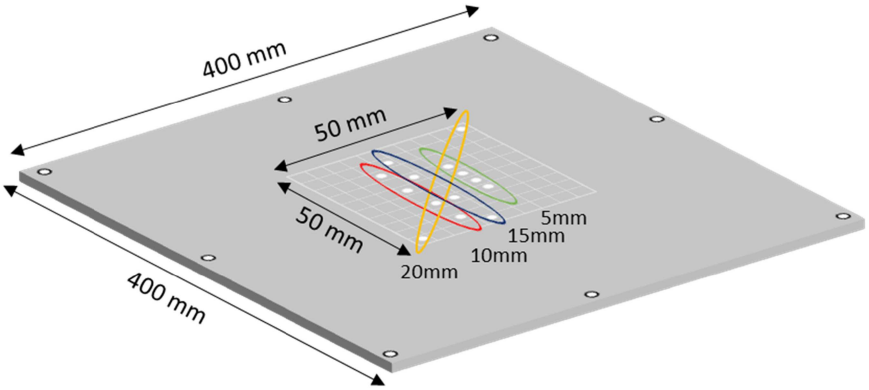

Figure 3. Aluminium clamping plates.

Figure 4. Pierced specimens with 15 mm hole spacing prior to OHT testing.

shown in Figure 2(a). For this work, only center-to-center spacings of 5, 10, 15, and 20 mm were considered for 2 mm diameter holes, and the arrangement of the pins is shown in Figure 2(b)–(e). The aluminum clamping plates were positioned above and below the laminate to be pierced; the plates incorporated the required hole spacings at the appropriate positions (see Figure 3). These plates provided support to the composite both during the heating stage and during piercing. Overall, the sequence for the specimen manufacture was as follows: (a) clamp the composite between the aluminium plates; (b) heat the composite and clamping plates to 200 °C (above the melting point of the PA12 matrix (≈180°C), to ensure sufficiently low melt viscosity and allow matrix flow during piercing); (c) the piercing rig is forced into the composite; (d) cool the laminate and clamping plates at a rate of approximately 2 °C/min (the piercing rig should be removed once the clamping plates reach room temperature); and (e) remove the pierced panel and cut the laminate into appropriate specimens. An example of a specimen with a hole spacing of 15 mm is shown in Figure 4.

2.2. Test methods

Current composite testing standards do not include provisions for specimens to have more than one hole, and consequently, the standards used for the tensile and Iosipescu tests adhered to the relevant standards (i.e. ASTM D5766/D5766M-11 and ASTM D5379/D5379M-19) [23,24], where possible. OHT testing was conducted on a minimum of ten specimens per hole spacing (i.e. five drilled and five pierced specimens); ten unperforated specimens were also tested. In the Iosipescu tests, fifteen specimens with two holes spaced 5 mm apart were tested (five drilled, five pierced and 5 unperforated). All tests were carried out using a 250 kN screw-driven Instron 8802 test frame. The OHT tests were performed at a crosshead speed of 2 mm/min, while the Iosipescu shear tests were conducted at a crosshead speed of 1 mm/min. The Iosipescu test fixture is shown in Figure 5.

The specimens were analysed using a combination of reflected light microscopy, three-dimensional surface profilometer and digital image correlation (DIC) measurements during loading. The optical microscopy images were acquired by using an inverted geometry optical microscope with a Colorview III camera (Olympus GX71). The specimen preparation for this technique included sectioning, grinding,

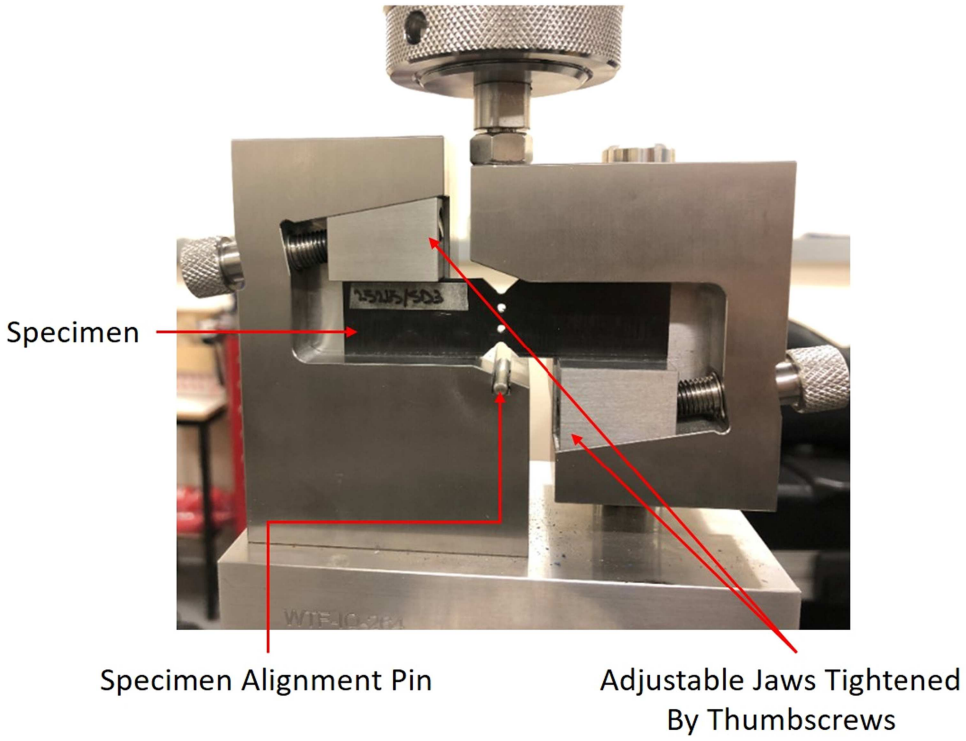

Figure 5. Drilled Iosipescu specimen placed in the test fixture.

and polishing the drilled and pierced specimens. For three-dimensional surface profilometry, an Alicona InfiniteFocus SL (focus variation microscopy) was used to understand the fiber distribution around the holes with the analysis performed using the associated IF Measure Suite software. The DIC technique was used to gather strain information in the vicinity of the drilled and pierced holes. The GOM-ARAMIS three-dimensional DIC system consisted of two cameras (controlled by ARAMIS software), and the system was set to record images at a frequency of 1 Hz during the tests. The analysis of the DIC data was conducted using GOM Correlate 2017 Professional after a surface component with a facet size of 19×19 pixels with 2 overlapping pixels was created. These settings are within the recommended parameters of the system and allow for a balance between accuracy and fast computation [25].

3. Results and discussion

3.1. Pierced specimen microstructural analysis

When a hole is drilled in a composite laminate, the resulting fiber distribution surrounding the hole remains unchanged, as shown schematically in Figure 6(a); the drilling process cuts the fibers rather than displacing them. When piercing a specimen, the fibers are deformed and displaced within the softened matrix, modifying the local material microstructure around the hole. In the plane of the laminate (shown schematically in Figure 6(b)), both the fiber volume fraction and fiber orientation are altered, but very few fibers breaks. The microstructure through the thickness is also altered significantly, and Figure 7 shows a section through the center of a hole, parallel to the 0° direction, and it is clear that plies are deformed in the through-thickness direction of the laminate as the piercing pin deforms the fibers and the molten matrix during piercing. The resultant effect of the TAP process is a fiber architecture that accommodates the deformation and displacement of the material as the piercing pin is forced through the laminate. The thinning of the plies towards the hole edge, and the formation of voids due to the flow of the molten matrix in conjunction with the fiber movement have also been previously observed in a carbon/PEEK composite [21].

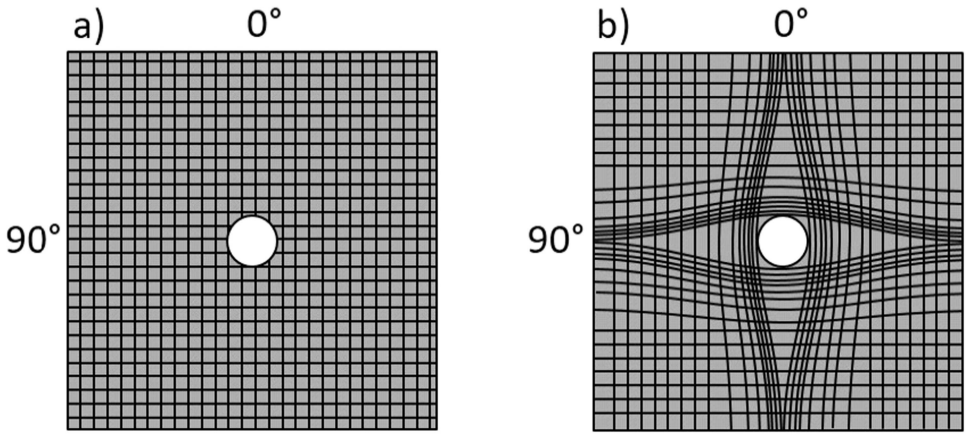

Figure 6. Schematic diagram of in-plane fiber architecture of holes for (a) drilled specimens and (b) pierced specimens.

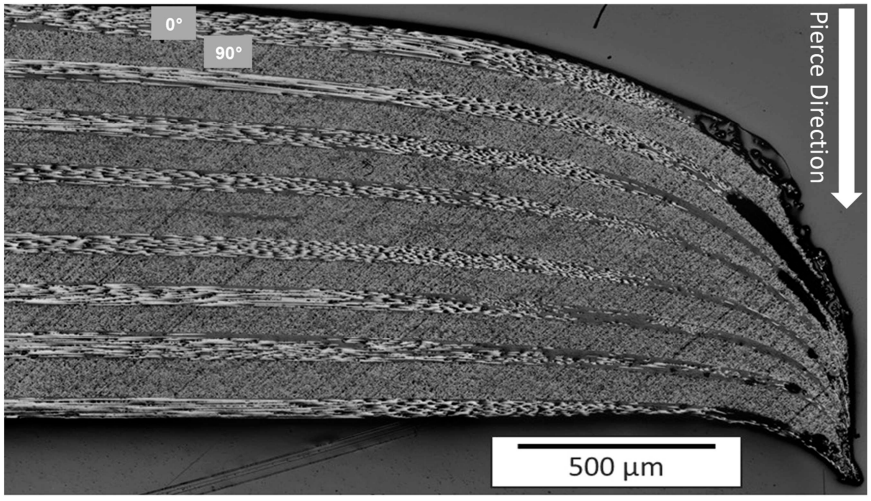

Figure 7. Optical microscopy image of the TAP specimen prior to testing, showing the 0° section cut after the TAP process. The white arrow shows the direction of the piercing pin.

Focus variation microscopy images, Figure 8, show clear changes in the path of the fibers around holes in the pierced specimens as a consequence of the piercing (obviously, there were no similar changes in the drilled specimens). The distance over which the fibers are distorted beyond the final hole in a line of four holes varied in the range of 1.5 hole diameters (i.e. 3 mm) to 3 hole diameters (6 mm), increasing from smaller hole spacings to larger hole spacings. Between the holes, the fibers return to their original path before piercing, provided that the holes are spaced sufficiently far apart. For the smallest hole spacing of 5 mm (Figure 8(a)), the fibers do not return to their original position, and it is possible that there has been significant fiber fracture due to large fiber strains imposed on the fibers between two holes in close proximity. These observations are reflected in the DIC results when the specimens are under load.

3.2. Strain distributions around multiple holes

The average loads to failure for each hole separation are shown in Table 1. The failure loads reported in Table 1 do not exhibit a monotonic dependence on hole spacing, with the 15 mm configuration showing a higher mean load to failure than both smaller and larger spacings in the present dataset. Figure 9 shows the DIC images for both (a) drilled and (b) pierced specimens for hole spacings of 20, 15, 10, and 5 mm, respectively. The DIC images were taken at various loads corresponding to approximately 60% of the load

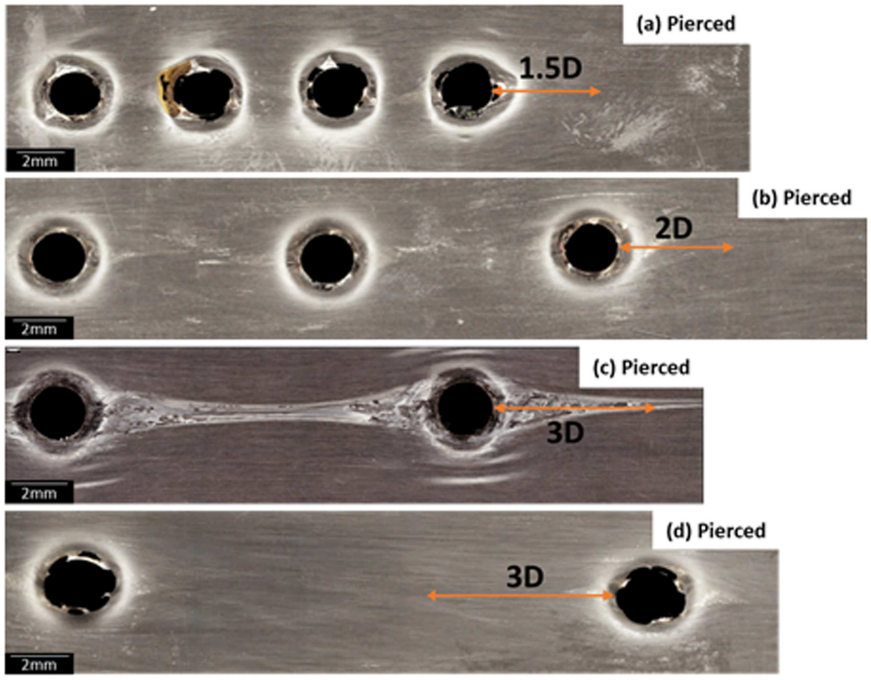

Figure 8. Infinite focus microscopy of the surface of pierced specimens for spacings of (a) 5 mm, (b) 10 mm, (c) 15 mm, and (d) 20 mm.

Table 1. Average load to failure. Values are reported as mean ± standard deviation (SD) ($n = 5$).

Specimen ID	Average load to failure (kN)	SD (kN)
20 mm_Drilled	25	±7
20 mm_Pierced	24	±15
15 mm_Drilled	32	±3
15 mm_Pierced	38	±6
10 mm_Drilled	27	±5
10 mm_Pierced	21	±8
5 mm_Drilled	27	±6
5 mm_Pierced	26	±5

to failure for each configuration. Figure 10 shows the DIC results for strain as a function of position, using virtual sections to show the variation in strain at various distances from the center line of the holes for both (a) drilled and (b) pierced specimens for the same hole spacing of 20, 15, 10, and 5 mm, respectively. This allows a direct comparison to be made between the drilled and pierced holes with respect to the strains measured along the virtual sections.

Figure 9(i)(a) and 9(i)(b) show the DIC results for the 20 mm hole separation for the drilled and pierced specimens, respectively. The background strain derived from the applied load and the Young's modulus of the material (the Young's modulus was measured to be 59 GPa ± 8 GPa, measured on unperforated specimens) corresponded to a strain of 0.57% for the drilled specimen and 0.51% for the pierced specimen. This is in good agreement with the background strain derived from the DIC measurements of 0.59% and 0.51%, respectively (Table 2).

Figure 9(i)(a) suggests that, between the drilled holes, the strain is much lower than the background strain, and although the same occurs for the pierced holes (Figure 9(i)(b)), it is clear that the pattern in the behavior of the strain is different. In order to examine the strain distributions in more detail, virtual sections were constructed, and the longitudinal strain was investigated as a function of position along each of these virtual sections. Figure 10 shows a schematic of each test piece along with color-coded lines indicating the location of the virtual sections (four for each specimen); the strain distribution for each virtual section is shown to the right of each of the schematics. For example, Figure 10(i)(a) and 10(i)(b) show the virtual section results for the drilled and pierced specimens of Figure 9(i)(a) and 9(i)(b); the same

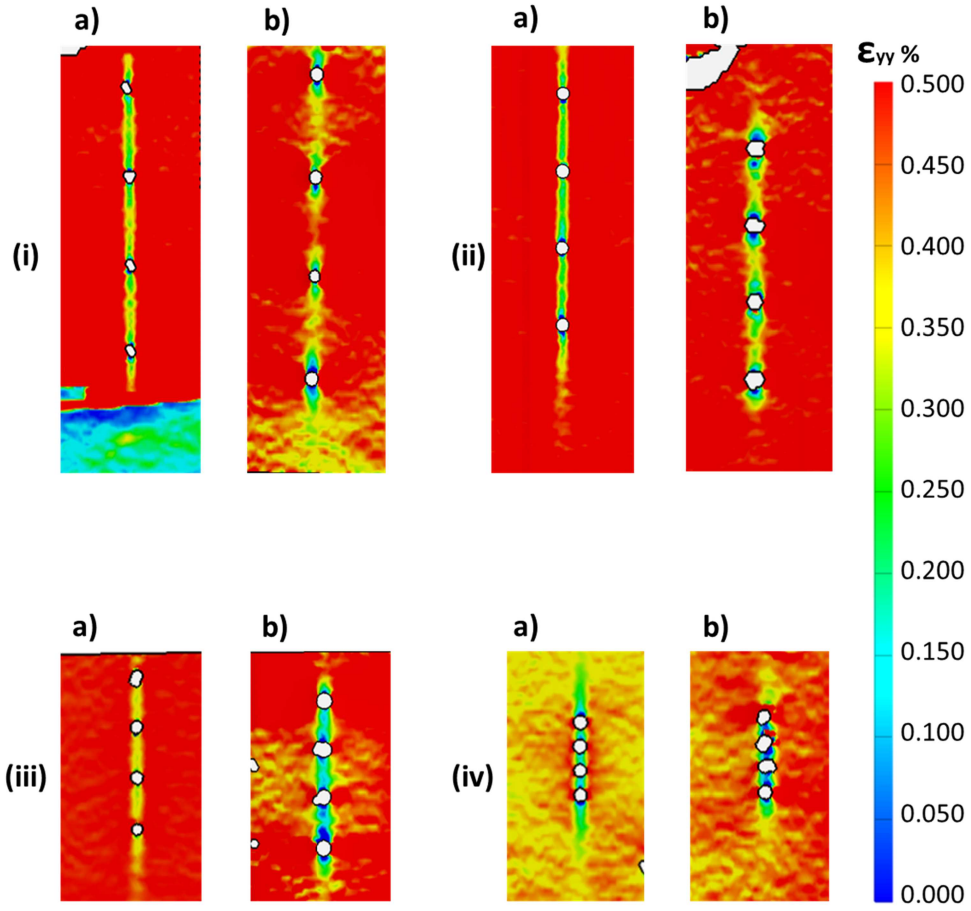

Figure 9. DIC images for the OHT test for four different hole separation group: (i) 20 mm, (ii) 15 mm, (iii) 10 mm, (iv) 5 mm, with (a) drilled and (b) pierced specimens.

is true for the other images in Figures 9 and 10. For all of the specimens, the virtual sections 1 and 4 were both 4 mm away from the hole edges on either side of the hole; virtual section 2 was 1.5 mm from the hole edge, and virtual section 3 was the line connecting the center of the holes. This ensured that the strain measurements were taken at the same locations for all the specimens.

In Figure 10(i)(a), which is related to the drilled holes with a spacing of 20 mm, virtual sections 1 and 4 show similar behavior. This would be expected since they are at the same distance, but on opposite sides, of the hole. They both show a similar average strain of approximately 0.55%, i.e. close to the background (i.e. applied) strain of 0.57%. The expression for the stresses around a hole in an isotropic material can be used to estimate what local increase in longitudinal strain might be expected 4 mm from the hole edge. Of course, since the expression is for an isotropic material, it will only be an approximation for this biaxially reinforced composite. At a distance of 5 mm from the center of the hole, the stress is expected to be only 2% higher than the nominal stress, since the stress is given by [26]:

$$\sigma_{yy} = \frac{\sigma_{nom}}{2}\left(2 + \frac{a^2}{x^2} + \frac{3a^4}{x^4}\right) \quad (1)$$

Here, the radius of the hole is $a = 1$ mm and x is the distance from the center of the hole in a direction at right angles to the direction of the nominal stress. For virtual sections 1 and 4, which are 4 mm from the hole edge, this corresponds to a distance $x = 5a$. Hence, it is not surprising that no significant increase in strain was detected in the DIC results for the drilled specimen at a distance of 4 mm from the hole edges. A similar behavior is observed in the pierced specimens, although there are local increases in strain in the vicinity of the hole, which presumably reflect the fiber distortions around the hole.

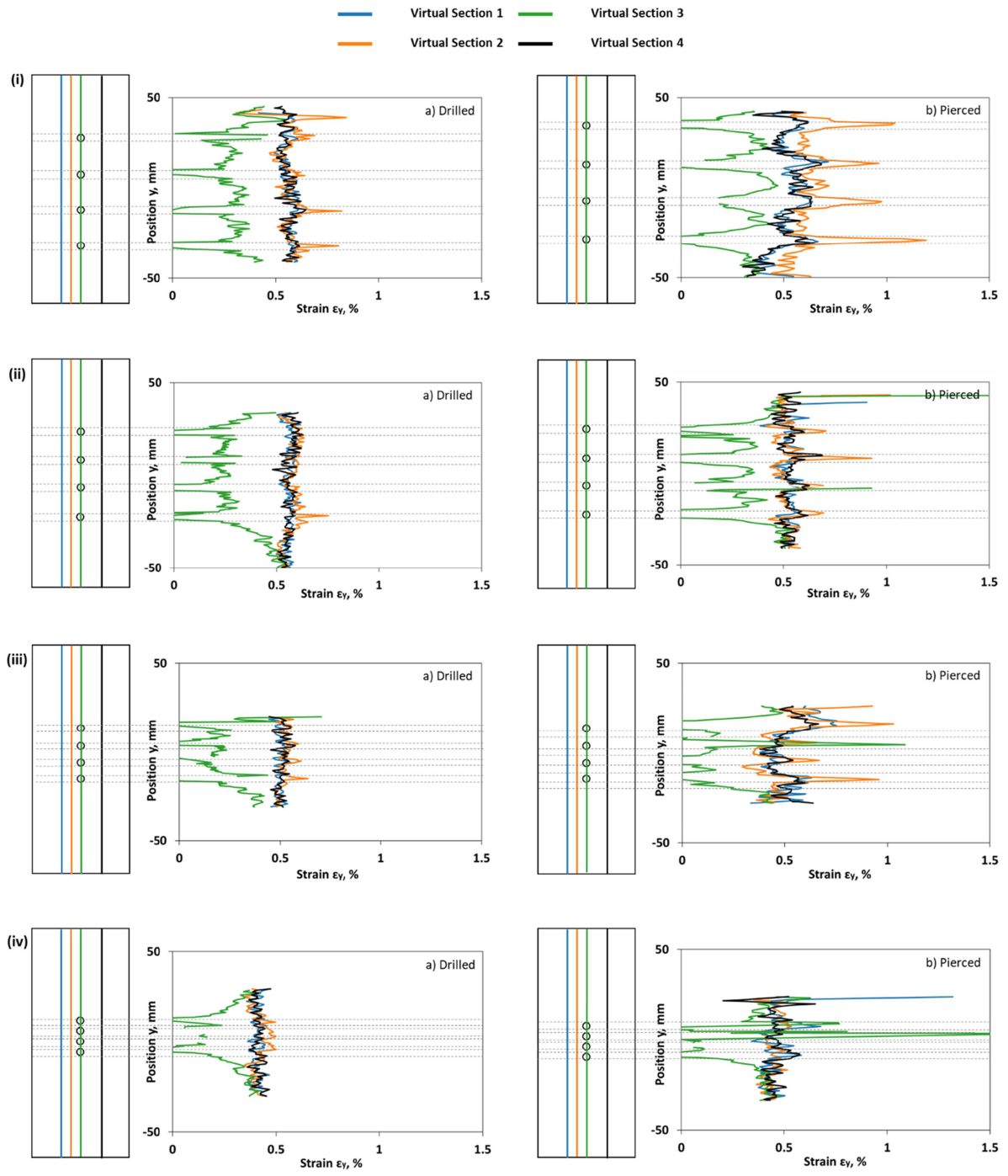

Figure 10. Longitudinal strain as a function of position for (i) 20 mm, (ii) 15 mm, (iii) 10 mm, (iv) 5 mm with (a) drilled and (b) pierced specimens.

Considering all of the hole spacings, for both drilled and pierced, Table 3 shows a comparison between the strain applied to the specimen (as shown by the DIC background strain) and the peak strain, which occurred in each case adjacent to the hole, in the virtual section. In all the cases, the peak strains adjacent to the holes for virtual sections 1 and 4 are approximately the same as the background strains, as expected.

In contrast, virtual section 2 is only 1.5 mm from the hole edge (i.e. $x = 2.5a$), and the nominal strain is expected to increase by approximately 12% in an isotropic material. Figure 10(i)(a) and Table 3 show that the local strain adjacent to the center of the hole for virtual section 2, for the holes spaced 20 mm apart, increases by approximately 13% for the drilled holes relative to the measured background strain, which is

Table 2. Applied and measured (DIC) background strain for the 20, 15, and 10 mm hole separation groups for both drilled and pierced specimens.

Specimen ID	Applied strain (%)	Average measured background strain (DIC) (%)
20 mm_Drilled	0.57	0.59
20 mm_Pierced	0.51	0.51
15 mm_Drilled	0.54	0.54
15 mm_Pierced	0.56	0.53
10 mm_Drilled	0.48	0.55
10 mm_Pierced	0.51	0.52

Table 3. Summary of the expected and measured strains for the drilled and pierced specimens at virtual Sections 1, 2, and 4. Sections 1 and 4 are 4 mm away from the hole edge. Section 2 is 1.5 mm away from the hole edge.

Specimen ID	Background strain DIC (%)	Section	Average peak strain for the virtual sections (%)
20 mm_Drilled	0.57	1 and 4	0.55
		2	0.67
20 mm_Pierced	0.51	1 and 4	0.52
		2	0.84
15 mm_Drilled	0.54	1 and 4	0.56
		2	0.58
15 mm_Pierced	0.56	1 and 4	0.53
		2	0.70
10 mm_Drilled	0.48	1 and 4	0.57
		2	0.64
10 mm_Pierced	0.51	1 and 4	0.53
		2	0.80

close to the prediction. However, for the pierced holes, the increase in local strain is much greater (approximately 66%). The higher local strain for the pierced holes is probably related to the local distortion of the fibers around the holes, leading to low modulus regions, particularly near the hole where the distortions of the fibers due to the piercing process are greatest. This effect, i.e. higher longitudinal strain adjacent to the hole in the pierced specimens, can also be seen in Figure 10(ii) and 10(iii) and for the other hole separations, i.e. 15 and 10 mm. The analysis of the strain results for 5 mm hole spacing has been excluded, as the strain results close to the holes are difficult to discern from the DIC data.

The much higher local strains adjacent to the holes along virtual section 2 for the pierced specimens, compared to the drilled specimens, can possibly be explained by considering the effect of the change in the fiber angle, as a consequence of the piercing process, on the local Young's modulus of the material. Fiber displacement during piercing takes place at 0° and 90° plies, both within the original fiber plane during piercing and, especially locally, through the composite thickness (Figures 7 and 8), all of which might be expected to reduce the local modulus of the material. The consequences of fiber distortion in 0° plies have been estimated using the compliance matrix approach [e.g. 27]. The matrix and fiber moduli ($E_m = 1.35$ GPa and $E_f = 231$ GPa) were taken from the CES Selector [28] and the supplier's datasheet [29], respectively. With a fiber volume fraction of $f = 0.55$, the longitudinal and transverse moduli of the unidirectional material are then $E_1 = 151$ GPa and $E_2 = 4.7$ GPa, respectively (using the Halpin–Tsai equations with $\xi = 1 + 40f^{10}$). Using standard micromechanics equations, then ν_{12} and ν_{21} are 0.3 and 0.03, with values for the fiber and matrix Poisson's ratios taken to be $\nu_f = 0.2$ and $\nu_m = 0.4$ [28]. Figure 11 shows the variation in the Young's modulus with loading angle for the unidirectional composite material. The focus variation microscope results showed that the fiber angle around the hole in the pierced composites can change by up to 10°–20°. Figure 11 suggests that this would lead to a local modulus reduction of approximately 70%–90% for the 0° plies in the loading direction; hence, it is not surprising that a much higher strain is found adjacent to the holes for virtual section 2 (i.e. close to the hole) in the pierced specimens, where fiber-bending occurs. A higher longitudinal strain adjacent to the center of the pierced holes can also be seen in Figure 10(ii) and 10(iii) for the 15 and 10 mm hole separation.

Considering the behavior of the strains along the virtual section 3 (which connects the hole centers), it can be seen from Figure 10 that the strain variations also differ considerably between the pierced and drilled specimens. Focusing again on the hole separation of 20 mm for both the drilled and pierced holes,

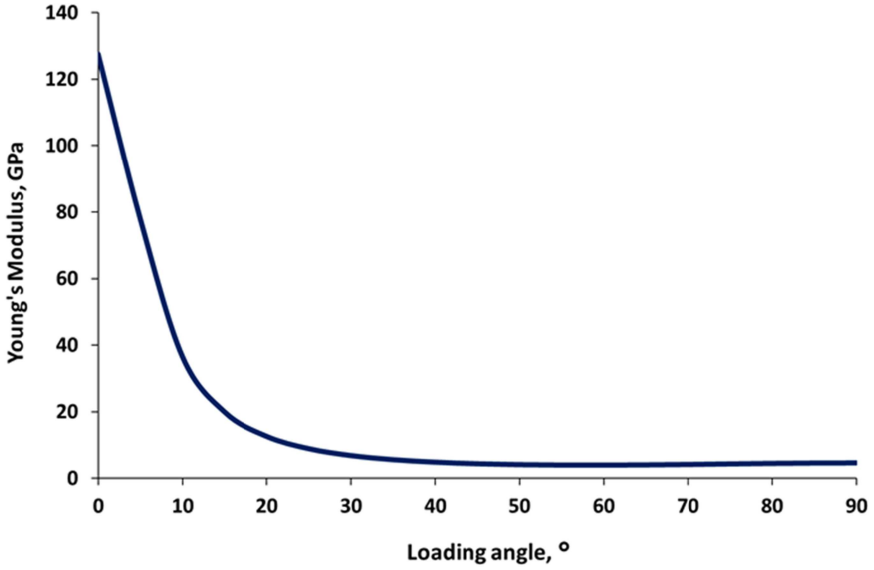

Figure 11. Variation with the loading angle of Young's modulus E_x, for CF/PA (fiber volume fraction of 55%).

Table 4. Measured and predicted [30] ratios of peak longitudinal strain between the holes to the applied strain; predictions are based on a model for stress build-up between two matrix cracks. The measured values are averages taken over the four holes in each coupon.

Specimen ID	Measured: peak strain/applied strain	Predicted: peak strain/applied strain
20 mm_Drilled	0.52	0.52
20 mm_Pierced	0.81	0.53
15 mm_Drilled	0.41	0.44
15 mm_Pierced	0.71	0.45
10 mm_Drilled	0.36	0.31
10 mm_Pierced	0.29	0.31

then the strain, ε_{yy}, decreases to zero at the location of the hole edges, as expected, but between the holes, the strain increases to a peak value. Table 4 shows the ratio of the peak strain to the applied strain for the drilled and pierced specimens. It is clear from Table 4 and Figure 10 that (a) for both drilled and pierced holes, the strain between the holes does not increase to the value of the background (applied strain) level; (b) the peak strain between the holes is generally greater for the pierced specimens compared to the drilled specimens; and (c) that the shape of the rise to the peak strain between the holes differs between the drilled and pierced holes. Table 4 also shows that the measured ratio of the peak strain between the holes to the applied strain is highest for the specimens with holes farthest apart (20 mm) and reduces when the hole spacing reduces for both 15 and 10 mm.

The build-up of the stress in between the holes can be understood reasonably well with the aid of a model originally devised to consider the behavior of stresses between two matrix cracks in the 90° ply of a cross-ply, i.e. (0/90/0), composite laminates [30]. Notably, this shear–lag model is used here as a first-order approximation to capture trends in strain build-up between holes. The assumption of a uniform modulus for all parts of the coupon (i.e. $E_0 = E_1 = E_2$; see below) is reasonable for the drilled specimens, since the fiber distribution and fiber orientations are not altered by the drilling process. However, this is not the case for the pierced specimens, where the piercing process introduces changes to the fiber distribution and fiber orientations.

Figure 12(a) shows a schematic of the edge of a (0/90/0) composite, which has an outer 0° plies with a thickness of b and a center 90° ply with a thickness of 2d. The cross-ply laminate has two through-thickness matrix cracks, A and B, a distance 2s apart. When the composite is subjected to an average stress σ_{nom} in the 0° direction, then the variation in stress, σ_2, between the cracks A and B at 90° ply is given by:

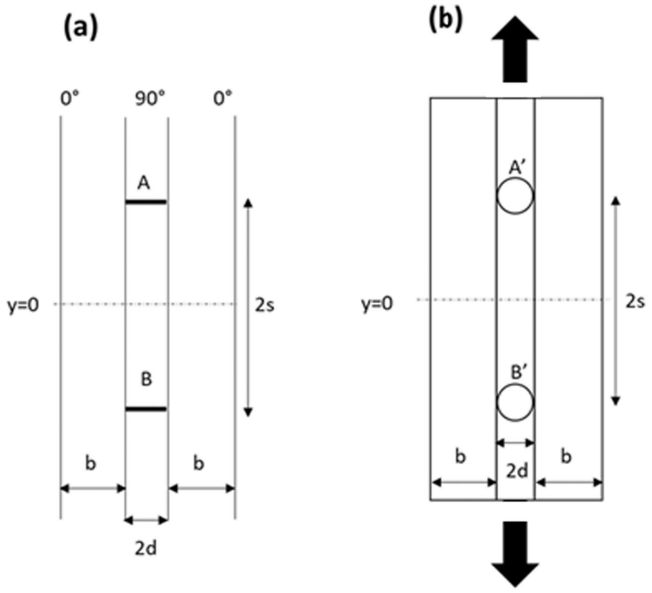

Figure 12. Schematic drawing of (a) geometry of cross-ply laminate (edge view) from the matrix crack model; A and B show the cracks, where 2s is the distance between the cracks, y = 0 is located halfway in between the cracks. (b) Geometry of the composite based on the matrix crack model; A′ and B′ show the holes, 2s is the distance between the holes, and y = 0 is located halfway in between the holes.

$$\sigma_2 = \sigma_{nom}\left(\frac{E_2}{E_0}\right)\left(1 - \left(\frac{cosh\left(\lambda y\right)}{cosh\left(\lambda s\right)}\right)\right) \tag{2}$$

Here, E_0 is the modulus of the laminate, E_2 is the modulus of the 90° ply, and the origin of the coordinates (i.e. $y = 0$) is mid-way between the cracks. The quantity λ is given by $\lambda^2 = \frac{\alpha G(b+d)E_0}{d^2 b E_1 E_2}$ (Boniface et al. 1991), where the value of α could be 1 or 3 (in this work, the value of 3 provided a better fit). This model can be applied to predict the build-up of stress between the holes in the CF/PA composite. Instead of cracks A and B, there are holes A' and B', and so the thickness of the central strip (the 90° ply in the matrix cracking model) is the diameter of the holes (i.e. 2 mm). For the CF/PA composite, the Young's modulus of the material between the holes and the Young's modulus of the rest of the composite are the same (unlike in the original matrix cracking model). Hence, the dimensions and properties to be used are: $2d = 2$ mm, $b = 17$ mm, $E_0 = E_1 = E_2 = 59$ GPa and $G \approx 0.6$ GPa; the value of the shear modulus was obtained from the Iosipescu shear tests (see below).

Equation (2) can now be used to predict the ratio of peak strain between the holes (i.e. at $y = 0$) compared to the background strain for drilled and pierced specimens, compared to experimental measurements of the same ratio (Table 4) (the ratio of the strains is the same as the ratio of the stresses since linear elasticity has been assumed); the strain measurements for the 5 mm holes are unreliable and so have not been included. As the spacing of the holes decreases from 20 to 10 mm, the predicted ratio of peak strain to applied strain decreases (note that the predictions for the drilled and pierced specimens for each particular hole spacing would be the same if the dimensions of the specimens were the same). There is reasonable agreement between the measured and predicted ratios for the drilled specimens. Similarly, the measured ratio also decreases, so the trends are correct.

However, the agreement between the measured strain ratios and the predicted strain ratios is worse for the pierced specimens, with the predicted ratios being considerably lower for the 20 and 15 mm. As indicated above, this is likely related to the perturbation of the fibers around the hole in the pierced specimens due to the piercing process. The shape of the rise to the maximum strain value between the holes differs between the pierced and drilled specimens. The focus variation microscopy results (Figure 8) show that the perturbations of the fiber positions as a consequence of piercing can occur up to a distance of approximately 6 mm (i.e. 3D) from the hole edges. This means that, as a consequence of the

perturbation of the fibers, the actual modulus of the material between the pierced holes is likely to be less than the modulus of the material with unperturbed fibers (Figure 11), producing a significant change in the peak strain between the holes. For example, a reduction in the value of the modulus of the composite between the holes by approximately 40% would lead to an approximately 35% increase in the peak strain. Of course, in general, the model cannot predict the behavior of the strains along virtual section 3 precisely (since the model was developed for a composite laminate with matrix cracks and not for a composite with an array of holes), but it does account reasonably well for the trend in the strains along virtual section 3.

Interestingly, the differences in the local strain distributions as determined by DIC did not lead to consistent differences in the strengths of drilled and pierced specimens. Figure 13 shows the tensile strengths for the unperforated, drilled, and pierced groups. A previous study [21] revealed that pierced specimens had a higher strength than drilled specimens, and this was also found here for specimens with hole spacings of 15 and 20 mm – i.e. the greater the hole spacing. However, for the smaller hole spacing of 10 mm, the drilled specimens had a higher strength, and for the 5 mm sample, there were insufficient data to draw a conclusion. The higher local strains measured adjacent to the TAP holes reflect a reduction in local stiffness caused by fiber distortion and misalignment introduced during the piercing process, rather than an increase in the local stress carried by intact fibers. As a result, these high-strain regions correspond to low-modulus zones and are not necessarily the locations governing tensile failure. In contrast, the preservation of fiber continuity in the TAP specimens enables load redistribution around the holes compared to drilled specimens, where fibers are severed. The tensile strength response, therefore, reflects a balance between two competing mechanisms, local modulus reduction, which increases the strain concentrations, and fiber continuity, which mitigates strength loss, with their relative influence depending on hole spacing.

3.3. Iosipescu test

For the shear experiments, four groups of specimens were tested: drilled CF/PA, pierced CF/PA, drilled PA, and unperforated PA; the drilled and pierced specimens had two holes each. Five specimens were tested in each group. The load-displacement responses for the four groups of specimens are shown in Figure 14. Data beyond a crosshead displacement of 2 mm was excluded from the analysis, as the fixture reached its displacement limit ('bottoms out'), which is consistent with the behavior described in the test standard. All of the drilled and unperforated specimens, both pure matrix and composites, showed a smoothly increasing load–displacement curve, but the pierced composite specimens showed an atypical response, with softening at approximately 0.35 mm crosshead displacement (which resembled a 'kink' in

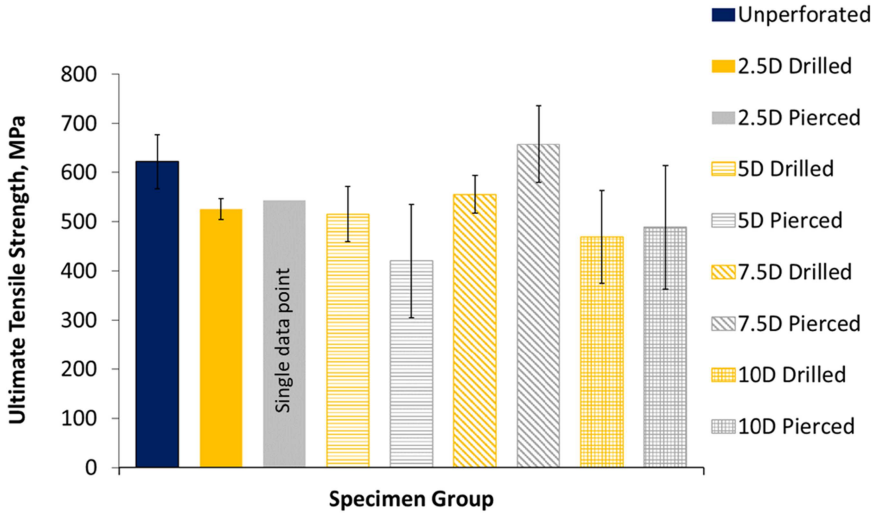

Figure 13. Average tensile strength of the composite for unperforated (UP), pierced (P), and drilled (D) groups. The error bars indicated plus/minus one standard deviation.

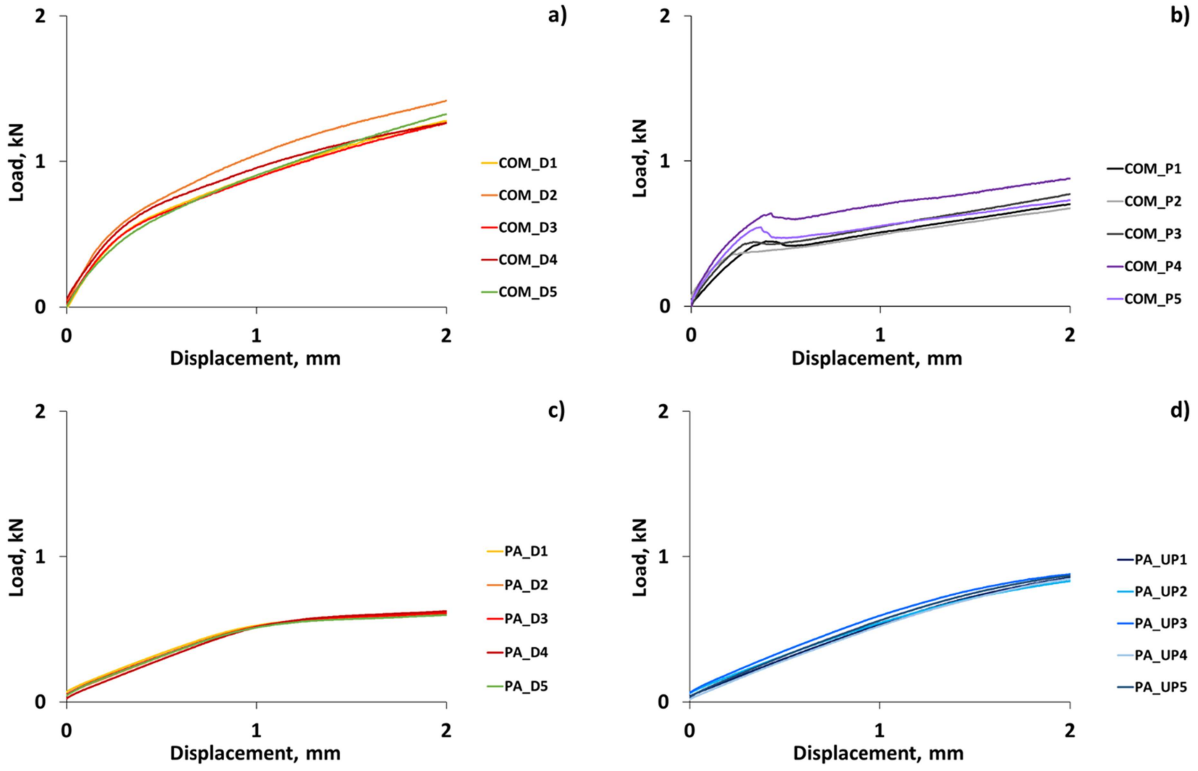

Figure 14. Load–displacement plots from the V-notched shear tests for (a) drilled CF/PA composite; (b) pierced CF/PA composite; (c) drilled PA matrix alone; and (d) unperforated PA matrix.

Table 5. Summary of the V-notched shear stress data for the drilled and pierced composite specimens, and the drilled and unperforated matrix specimens. Values are reported as mean ± standard deviation (SD).

	Composite drilled	Composite pierced	Matrix drilled	Matrix unperforated
Stress at 2 mm crosshead displacement, MPa	50 ± 4	27 ± 3	17 ± 1	24 ± 0.1

the load-displacement curve (Figure 14(b))), followed by a linear region. The origin of this softening behavior is discussed below.

The Iosipescu load-displacement data were converted to shear stress/shear strain. In the case of the specimens with holes, the net section stress was used, i.e. for two holes with a diameter of 2 mm, where there was a distance between the notches of 11.4 mm, which means that the load was effectively carried over an area reduced to 65% of the original cross-sectional area (i.e. a 35% reduction). The shear modulus of the PA-12 matrix was 0.48 GPa ± 0.04 GPa for the unperforated group of specimens and 0.43 GPa ± 0.03 GPa for the drilled group of specimens. Both of these values are in good agreement with the CES Selector [28] value of 0.4 GPa. For the CF/PA composite specimens, the shear modulus was similarly derived from the shear stress/shear strain data, although tests were only carried out on drilled and perforated specimens (and not on unperforated specimens). The shear modulus was 0.6 GPa ± 0.2 GPa for the drilled group of specimens and 0.8 GPa ± 0.2 GPa for the pierced group of specimens. The values were calculated over the pre-kink region.

The Iosipescu tests did not allow the shear strength to be determined for the composites because of the bottom-out of the fixture. Hence, in order to compare the resistance to deformation of the various groups of specimens, the stress values were compared for a 2 mm crosshead displacement. Table 5 shows a summary of the Iosipescu shear strength data for the four groups of specimens. The drilled composite specimens showed a 46% higher average stress (at a displacement of 2 mm) in comparison to the pierced composite specimens, and further investigation revealed the reasons for these differences.

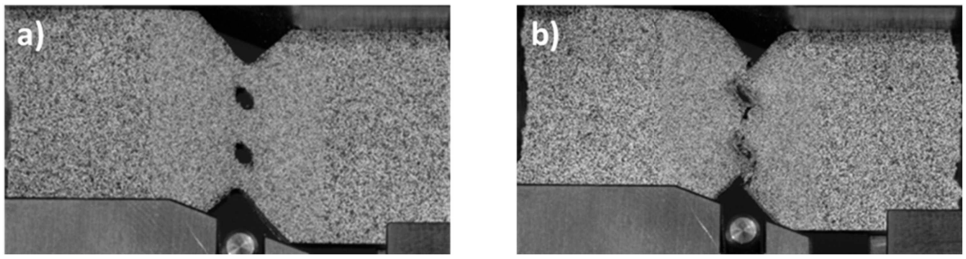

Figure 15. V-notched specimens at 90% of the maximum load for (a) drilled and (b) pierced specimens.

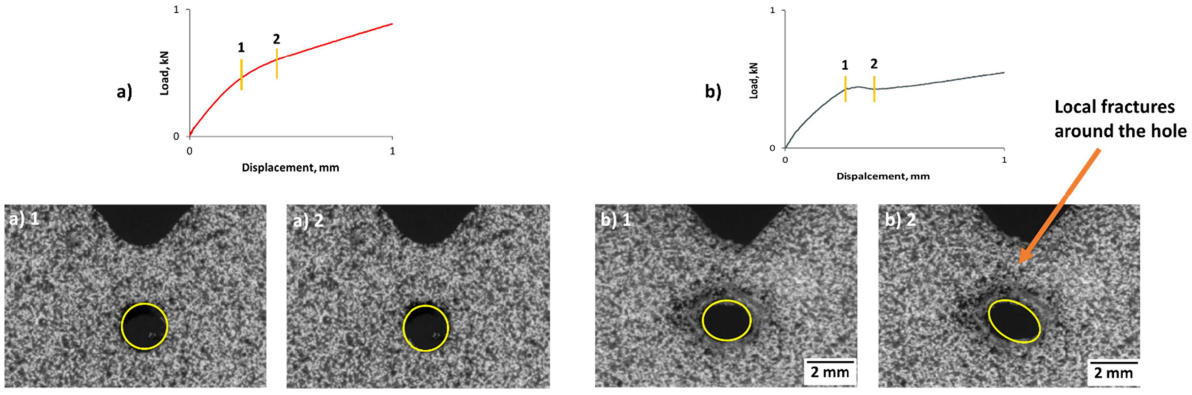

Figure 16. Comparison of (a) drilled and (b) pierced holes at 0.3 and 0.47 mm displacement, showing significant damage and hole shape-change for the pierced hole compared to the drilled hole.

Figure 15 shows examples of (a) drilled and (b) pierced specimens at 90% of the maximum load measured for each type of specimen (i.e. 90% of the load for a 2 mm displacement). By this point, the pierced holes (Figure 15(b)) have collapsed completely, whereas the holes in the drilled specimens have deformed only to an elliptical shape. The premature collapse of the pierced holes under shear loading is preceded by significant early damage (discussed below).

Figure 16 shows examples of (a) a drilled hole and (b) a pierced hole for the same crosshead displacements of 0.3 mm and 0.47 mm (i.e. just before, and just after, the softening in the load-displacement curves for the pierced specimens). The yellow circles and ellipses in Figure 16 delineate the hole shapes. For the drilled hole, there is essentially no change in the shape of the hole over this displacement range. In contrast, for the pierced hole, the hole is circular before softening in the load-displacement curve but has collapsed to an elliptical shape after softening. The change in shape is accompanied by evidence of local fracture above and below the hole in regions associated with fiber rearrangement and resin-rich areas resulting from the piercing process. The subsequent collapse of the holes in the pierced specimens may be caused by a combination of the local softening due to cracking damage and the intact fibers around the hole pulling material towards the hole. Figure 17 shows displacement vectors determined using DIC for the (a) drilled and (b) pierced composite specimens taken at 2 mm crosshead displacement. Surface points were created on the surface components of the DIC images, and the points were then used to obtain information regarding their displacement direction under loading. The displacement vectors for the drilled holes (Figure 17(a)) show the displacements that would normally be expected in an Iosipescu shear test, with the two regions of the specimen to the left and right displacing independently of each other. However, for the pierced specimen, the displacement vectors seem to suggest that the continuous fibers are causing displacements in the direction of the hole, which is likely to be the reason why the pierced holes collapse. Similar observations on unreinforced PA-12 specimens showed that the holes deformed in a similar way to the drilled composites, i.e. the holes did not collapse.

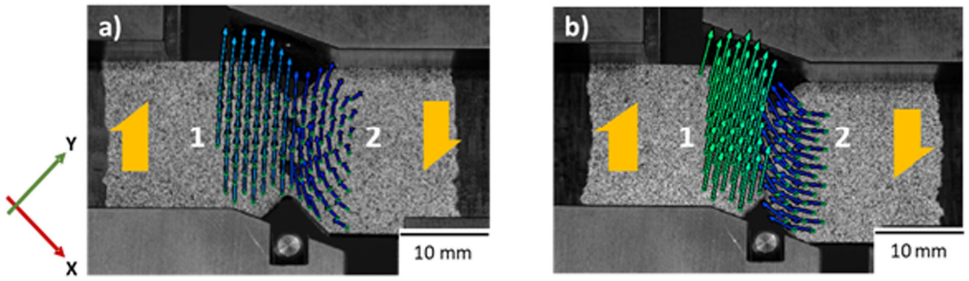

Figure 17. Displacement vectors for (a) drilled and (b) pierced specimens at 90% of the maximum load.

Table 6. Summary of OHT results and representative DIC strain metrics for drilled and pierced specimens.

Hole spacing (mm)	Method	Average load to failure (kN) ± SD	Background strain (DIC) (%)	Peak strain at section 2 (DIC) (%)
20	Drilled	25 ± 7	0.57	0.67
20	Pierced	24 ± 15	0.51	0.84
15	Drilled	32 ± 3	0.54	0.58
15	Pierced	38 ± 6	0.56	0.70
10	Drilled	27 ± 5	0.48	0.64
10	Pierced	21 ± 8	0.51	0.80
5	Drilled	27 ± 6	–	–
5	Pierced	26 ± 5	–	–

Table 7. Summary of Iosipescu shear results reported as shear stress at 2 mm crosshead displacement. Values are reported as mean ± standard deviation (SD).

Specimen group	Stress at 2 mm crosshead displacement (MPa)
Composite – Drilled	50 ± 4
Composite – Pierced	27 ± 3
Matrix – Drilled	17 ± 1
Matrix – Unperforated	24 ± 0.1

Tables 6 and 7 summarizes the key findings from the OHT and Iosipescu shear results to facilitate comparison between the drilled and pierced specimens. The values were taken from Tables 1, 3, and 5.

4. Conclusions

Microscopy, tensile and Iosipescu shear testing, and DIC strain measurements were carried out on specimens of carbon fiber/PA12 that have been multiply-pierced using thermally assisted piercing. Surface observations using infinite focus microscopy have shown that fiber distortion as a consequence of multiple thermal piercing of the composites can extend up to 6 mm from the edge of a thermally pierced hole for a hole diameter of 2 mm. This rearrangement of the fibers, leading to regions of enhanced and reduced fiber volume fractions, causes significant differences in the local strain distributions around in-line holes under tensile loading. DIC observations of virtual sections parallel to the direction of the holes showed no significant strain changes 4 mm from the hole edges for the drilled specimens, but local increases in strain adjacent to the holes for the pierced specimens because of the local distortion of the fibers around the holes, which led to low modulus regions. For a virtual section 1.5 mm from the hole edge, the strain changes in the drilled holes adjacent to the holes are in line with what would be expected for a circular stress concentration, but again, the local strains are much higher for the pierced holes. For virtual sections taken between the hole centers, a shear–lag analysis originally developed for cross-ply composite laminates describes reasonably well the behavior of the peak strain (or peak stress) between the holes as a function of hole spacing; again, the peak strain is higher for the pierced specimens because of a lower modulus arising from the perturbation of the fibers caused by piercing.

Interestingly, despite the differences in the strains around the holes for pierced and drilled specimens, there was no consistent trend with regard to strengths for different hole spacings. For the Iosipescu shear

tests, the drilled specimens showed a significantly higher strength than that measured after a 2 mm cross-head displacement. The poorer performance of the thermally-pierced holes in shear is related to the premature collapse of the holes as a consequence of a combination of localized cracking in resin-poor areas and the action of the intact fibers being pulled across the holes, causing hole collapse.

Disclosure statement

The authors report there are no competing interests to declare.

Funding

This project has received funding from the University of Surrey as part of the EPSRC under the grant number of EP/GO37388/1, European Union's Horizon 2020 research and innovation programme under grant agreement No. 723360, and the Industrial Members of TWI Ltd. as part of the Core Research Programme.

ORCID

Faranak Bahrami 0000-0002-9491-166X

Data availability statement

The authors confirm that the data supporting the findings of this study are available within the article [and/or] its supplementary materials.

References

[1] Aerospace Manufacturing. Know the drill. Aerospace manufacturing. 2012. Available at: Know the drill (accessed 13 September 2017). https://www.aero-mag.com/know-the-drill
[2] Young T. Investigations into the operational effectiveness of hybrid laminar flow control aircraft. UK: PhD Thesis, University of Cranfield; 2002.
[3] Krishnan K, Seibel O. Review of hybrid laminar flow control systems. Prog Aerosp Sci. 2017;93:24–52. doi: 10.1016/j.paerosci.2017.05.005
[4] Ramkumar J, Aravindan S, Malhotra S, et al. An enhancement of the machining performance of GFRP by oscillatory assisted drilling. Int J Adv Manuf Technol. 2004;23(3-4):240–244. doi: 10.1007/s00170-003-1660-8
[5] Hocheng H, Tsao C. The path towards delamination-free drilling of composite materials. J Mater Process Technol. 2005;167(2-3):251–264. doi: 10.1016/j.jmatprotec.2005.06.039
[6] Khan Z, Mahmood A, Mills B, et al. The drilling-induced failure mechanisms in T800/924C toughened carbon-epoxy composite materials. J Reinf Plast Compos. 2013;33(2):202–211. doi: 10.1177/0731684413503510
[7] Durão L, Tavares J, de Albuquerque V, et al. Drilling damage in composite material. Materials. 2014;7(5):3802–3819. doi: 10.3390/ma7053802
[8] Panchagnula K, Palaniyandi K. Drilling on fiber reinforced polymer/nanopolymer composite laminates: a review. J Mater Res Technol. 2018;7(2):180–189. doi: 10.1016/j.jmrt.2017.06.003
[9] Torres M, Gonzalez JL, Hernandez H. Residual strength and fracture path fordrilled epoxy–glass composites. Adv Mater Res. 2009;65:89–96. doi: 10.4028/www.scientific.net/AMR.65.89
[10] Kumar D, Singh KK, Zitoune R. Experimental investigation of delamination and surface roughness in the drilling of glass fiber reinforced polymer (GFRP) composite material with different drills. Adv Manufact: Polym Compos Sci. 2016;2(2):47–56. doi: 10.1080/20550340.2016.1187434
[11] Composites World. 2012. Airbus delays A350 XWB by three months. Available at: (accessed 20 January 2017). http://www.compositesworld.com/news/airbus-delays-a350-xwb-by-three-months
[12] Barroeta Robles J, Dubé M, Hubert P, et al. Repair of thermoplastic composites: an overview. Adv Manufact: Polym Compos Sci. 2022;8(2):68–96. doi: 10.1080/20550340.2022.2057137
[13] Chang LW, Yau SS, Chou TW. Notched strength of woven fabric composites with moulded-in holes. Composites Part A. 1987;18(3):233–241. doi: 10.1016/0010-4361(87)90413-7
[14] Hufenbach WA, Gottwald R, Kupfer R. ICCM 18. 2011. Bolted joints with moulded holes for textile thermoplastic composites. Jeju, Korea; Proceedings of the 18th International Conference on Composite Materials (ICCM-18). paper no. M 6-20IF0724.
[15] Hufenbach W, Adam F, Winkler A. Technical Report (Collaborative Research Centre SFB 639, Subproject E1). Dresden, Germany: Technische Universität Dresden; 2012.

[16] Hufenbach W, Kupfer R, Horning A. Thermoactivated pinning – a novel joining technique for thermoplastic composites. Solid State Phenom. 2012b;188:176–181. doi: 10.4028/www.scientific.net/SSP.188.176
[17] Hufenbach W, Adam F, Körner I, et al. Combined joining technique for thermoplastic composites with embedded sensor networks. JIMSS. 2013;24(10):1226–1232. doi: 10.1177/1045389X12471870
[18] Ng SP, Tse PC, Lau KJ. Progressive failure analysis of 2/2 twill weave fabric composites with moulded-in circular hole. Composites: Part B. 2001;32:139–152. doi: 10.1016/S1359-8368(00)00040-8
[19] Zitoune R, Crouzeix L, Collombet F, et al. Behaviour of composite plates with drilled and moulded hole under tensile load. Compos Struct. 2011;93(9):2384–2391. doi: 10.1016/j.compstruct.2011.03.027
[20] Noda J, Imamura G, Ren B. Proceedings of the 15th European Conference on Composite Materials (ECCM-15). Venice, Italy; 2012. Development and mechanical properties of open-holed CFRP with non-cut fibers.Venice, Italy.
[21] Brown N, Worrall C, Ogin SL, et al. Investigation into the mechanical properties of thermoplastic composites containing holes machined by a thermally-assisted piercing (TAP) process. Adv Manufact: Polym Compos Sci. 2015;1(4):199–209.
[22] Hendley N. Making holes with helical interpolation. 2018. Available at: (accessed 1 September 2020). https://www.canadianmetalworking.com/canadianmetalworking/article/cuttingtools/making-holes-with-helical-interpolation
[23] ASTM D5766/D5766M-11: 2011. Standard test method for open-hole tensile strength of polymer matrix composite laminates.
[24] ASTM D5379/D5379M-19: 2019. Standard for test method for shear properties of composite materials by the V-notched beam method.
[25] GOM ARAMIS: User manual – Software (v6.3). 2007.
[26] Pilkey W, Pilkey D. Peterson's stress concentration factors. 3rd ed. John Wiley & Sons, Inc; 2007.
[27] Hull D, Clyne TW. An introduction to composite materials. 2nd ed. Cambridge, UK: Cambridge University Press; 1996. p. 56–73.
[28] Granta design Ltd, CES selector, materials selection software. Cambridge, UK: Granta Design Ltd; 2020.
[29] Hexcel Corporation HexTow® AS4 carbon fiber: product data sheet. Stamford, CT, USA: Hexcel Corporation; 2010.
[30] Boniface L, Ogin SL, Smith PA. Strain energy release rates and the fatigue growth of matrix cracks in model arrays in composite laminates. Proc R Soc A. 1991;432:427–444. doi: 10.1098/rspa.1991.0024